Direct and third-body mediated resonance energy transfer in dimensionally constrained nanostructures

Dilusha Weeraddana[*] and Malin Premaratne[†]
Advanced Computing and Simulation Laboratory (AχL), Department of Electrical and Computer Systems Engineering, Monash University, Clayton, Victoria 3800, Australia

David L. Andrews[‡]
School of Chemistry, University of East Anglia, Norwich Research Park, Norwich NR4 7TJ, United Kingdom
(Received 4 March 2015; revised manuscript received 13 May 2015; published 14 July 2015)

The process of resonance energy transfer (RET) in a nanostructure influenced by a vicinal, nonabsorbing third body is studied within the framework of molecular quantum electrodynamics. Direct RET and the influence of neighboring matter have been studied previously, mainly for molecules. However, a complete study or unified understanding of direct and indirect RET in nanostructures with different dimensionalities is still lacking. Therefore, there is a strong need for a complete theory that models RET for the cases of quantum wells, nanowires, and quantum dots. We construct a detailed picture of excitation energy transfer in nanostructures and how it is affected by another quantum object, which includes the derivation of quantum amplitudes based on second- and fourth-order time-dependent perturbation theories, and the derivation of transfer rates and distance dependencies, providing a complete picture and understanding of RET in nanostructures. The results of the derivations indicate that the dimensionality of the nanostructure determines the controllability of the RET rate. Furthermore, third-body mediation leads to a nonvanishing RET in the coupling of nanowire to nanowire and quantum dot to quantum dot.

DOI: 10.1103/PhysRevB.92.035128 PACS number(s): 31.30.J−, 78.70.−g, 33.50.Hv, 78.67.De

I. INTRODUCTION

Resonance energy transfer (RET), also often known as electronic energy transfer (EET), is a process in which electronic energy may be transferred nonradiatively between basic building blocks such as atoms and molecules, as well as functional blocks such as quantum wells (QWs), nanowires (NWs), or quantum dots (QDs). RET is well known to play an important role in the photodynamics of multichromophoric assemblies, and it mediates the storage and migration of energy in photosynthetic systems [1,2]. This has spawned recent interest in artificial light harvesting antenna devices [3–9] and nanoemitters, especially spasers [10]. Moreover, the process plays a vital role in biological science [11], where it is used mainly to determine either interactions or conformational dynamics within large biological structures [12], through its use as a spectroscopic ruler [13]. The electrodynamic mechanism and rate features of resonance energy transfer are now known for all internuclear separation distances R, beyond wave-function overlap and extending out to infinity. In the near zone, where R is much smaller than the wavelength, the well-known theory that enables the efficiency of RET to be predicted was proposed by Förster [14] in 1948. The significance of Förster's formulation is that it yields a rate of RET proportional to the inverse sixth power of distance in the near-field regime. Although the Förster energy transfer mechanism remains the most precise and widely employed concept in molecular energy transport, its deviations under some conditions have been often studied over the past few decades [15–18].

Since RET processes are fully quantum mechanical in nature, they can be formally described within the framework of quantum electrodynamics (QED). Within the context of QED, both matter and radiation are quantized and together they constitute a closed quantum mechanical system. Here, the RET process is mediated by the intermolecular propagation of virtual photons [19,20]. Although energy conservation is satisfied between the start and the end of the process, the intermediate state may violate the law of conservation of energy. This is entirely consistent with the time-energy uncertainty principle, and is usually illustrated by Feynman diagrams [21,22].

The development of a QED theory of RET, pioneered by Avery, Gomberoff, and Power [23,24], and continued by Craig and Thirunamachandran [20], culminated in a unified theory by Andrews [25,26]. Although the basic principles of RET are well established, there still exist open questions regarding the mechanisms of the RET phenomenon in many aspects. One of the important issues is to study RET in nanostructures of different dimensionalities. Moreover, introducing additional quantum objects to the system can significantly modify the RET efficiency. In this paper we specifically focus on the influence of a third functional building block (e.g., QDs or nanowires) when two particles exchange energy through a RET process.

The third-body mediated RET for basic building blocks, where the neighboring matter relays energy between the transmitter and receiver, has been previously studied in Refs. [27–31]. Nevertheless, modifying the electromagnetic (EM) modes according to the dimensionality [32,33] of the nanostructure should impose a degree of controllability over the RET efficiency. Our main aim in this paper is to construct

[*]dilusha.weeraddana@monash.edu
[†]malin.premaratne@monash.edu
[‡]d.l.andrews@uea.ac.uk

 ©2015 American Physical Society

a detailed picture of how individual photon behavior is modified by vicinal, nonabsorbing quantum objects such as QWs, NWs, and QDs. We seek to discover what particular effects arise in the matrix element and transfer rate when the input excitation is located in the neighborhood of other constitutionally different nanostructures, in terms of atomic transition frequency and relative distance. In Sec. II of this paper, the background molecular QED theory of RET is reviewed for both direct and indirect (third-body modified) energy transfer. In Secs. III and IV, direct and indirect RET for three types of nanostructures are presented. Results are discussed in Sec. V, followed by the conclusions in Sec. VI.

II. MOLECULAR QUANTUM ELECTRODYNAMICAL FORMALISM

The RET process is initiated by an excited donor which transfers energy to an acceptor because of the Coulomb interaction between transition dipoles in the donor-acceptor pair. A typical schematic illustration of the basic energy transfer process is shown in Fig. 1. In the multipolar formulation of molecular QED, the Hamiltonian for the radiation-matter system can generally be written as [20,34]

$$H_{\text{total}} = \sum_{\xi} H_{\text{int}}(\xi) + \sum_{\xi} H_{\text{mol}}(\xi) + H_{\text{rad}}. \tag{1}$$

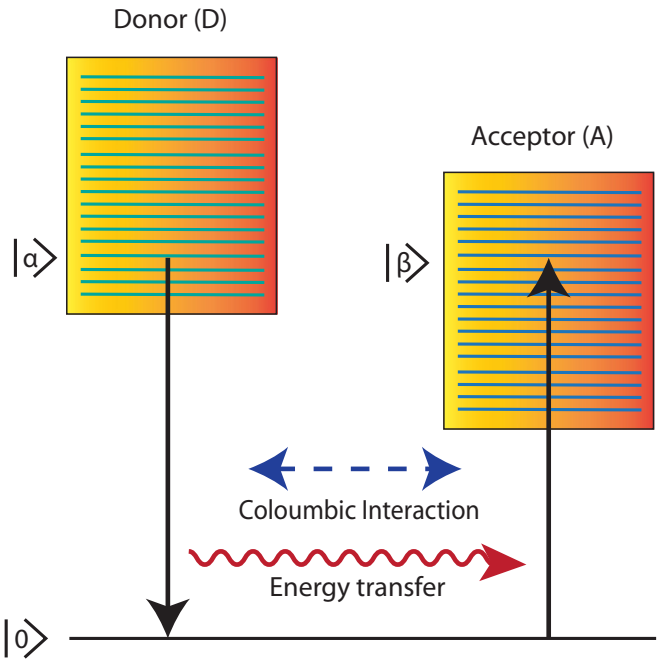

FIG. 1. (Color online) Schematic depiction of energy transfer from donor to acceptor. The black solid arrows represent emission and absorption of energy. The horizontal blue dashed arrow illustrates the Coulomb interaction between the donor and the acceptor. The horizontal red solid arrow represents the energy transfer from the donor to the acceptor. The Greek letters indicate the relevant electronic excited states and 0 the ground state.

The radiation-matter interaction is described using the multipolar Hamiltonian in the dipole approximation [20]

$$H_{\text{int}} = \sum_{\xi} -\boldsymbol{\mu}(\xi) \cdot \boldsymbol{E}(\boldsymbol{R}_{\xi}), \tag{2}$$

where the interaction Hamiltonian compromises contributions for each species ξ located at $\boldsymbol{R}_{\xi}$, the $\boldsymbol{\mu}(\xi)$ is the electric-dipole moment operator, and the electric field operator is given by $\boldsymbol{E}(\boldsymbol{R}_{\xi})$. The operator $H_{\text{mol}}(\xi)$ is the molecular Hamiltonian in the nonrelativistic Born-Oppenheimer approximation and H_{rad} is the second-quantized radiation field Hamiltonian.

The probability amplitudes for direct and indirect processes can both be derived from the time-dependent perturbation series

$$\begin{aligned} M_{FI} = {} & \langle F|H_{\text{int}}|I\rangle + \sum_{R} \frac{\langle F|H_{\text{int}}|R\rangle\langle R|H_{\text{int}}|I\rangle}{E_I - E_R} \\ & + \sum_{R,S} \frac{\langle F|H_{\text{int}}|R\rangle\langle R|H_{\text{int}}|S\rangle\langle S|H_{\text{int}}|I\rangle}{(E_I - E_R)(E_I - E_S)} \\ & + \sum_{R,S,T} \frac{\langle F|H_{\text{int}}|T\rangle\langle T|H_{\text{int}}|S\rangle\langle S|H_{\text{int}}|R\rangle\langle R|H_{\text{int}}|I\rangle}{(E_I - E_R)(E_I - E_S)(E_I - E_T)} \\ & + \cdots, \end{aligned} \tag{3}$$

where I,F are initial and final states, respectively, and R,S,T denote intermediate states. If $\zeta = I,F,R,S,T$, then E_{ζ} denotes the corresponding eigenenergy. The fundamental process of direct RET, the migration of energy between the donor (D) and acceptor (A), corresponds to the process

$$D^{\alpha} + A^{0} \longrightarrow D^{0} + A^{\beta}.$$

Here, the superscripts denote the donor and acceptor states. This coupling is mediated by a virtual photon. When the interaction-pair separation is relatively small and within the Förster range, the photon time of flight becomes small, resulting in a large uncertainty in the system energy. Nevertheless, as the separation of the interaction pair increases, this uncertainty is reduced, effectively imposing on the virtual photon an increasingly real character until the virtual characteristics become indistinguishable [19]. The virtual photon can be created either at the donor or acceptor. Therefore, the quantum amplitude M_{FI}^{d} is calculated from the second term in the time-dependent perturbation series explicitly given as follows, with the superscript d on the left denoting "direct":

$$M_{FI}^{d} = \frac{\langle F|H_{\text{int}}|R_1^1\rangle\langle R_1^1|H_{\text{int}}|I\rangle}{E_I - E_{R_1^1}} + \frac{\langle F|H_{\text{int}}|R_1^2\rangle\langle R_1^2|H_{\text{int}}|I\rangle}{E_I - E_{R_1^2}}. \tag{4}$$

To represent the energy transfer from donor to acceptor, the initial, final, and intermediate matter-radiation state vectors are chosen to be the following eigenvectors with corresponding eigenenergies [26],

$$|\Psi_I\rangle = |D^{\alpha}A^{0};0(\mathbf{p},\lambda)\rangle, \quad E_I = E_{\alpha}^{D} + E_{0}^{A}, \tag{5}$$

$$|\Psi_F\rangle = |D^{0}A^{\beta};0(\mathbf{p},\lambda)\rangle, \quad E_F = E_{0}^{D} + E_{\beta}^{A}, \tag{6}$$

$$|\Psi_{R_1^1}\rangle = |D^{0}A^{0};1(\mathbf{p},\lambda)\rangle, \quad E_{R_1^1} = E_{0}^{D} + E_{0}^{A} + \hbar cp, \tag{7}$$

$$|\Psi_{R_1^2}\rangle = |D^{\alpha}A^{\beta};1(\mathbf{p},\lambda)\rangle, \quad E_{R_1^2} = E_{\alpha}^{D} + E_{\beta}^{A} + \hbar cp, \tag{8}$$

with the energy identity

$$E^D_{0\alpha} = E^A_{\beta 0} = \hbar ck, \tag{9}$$

where $\boldsymbol{p}$ is the photon wave vector, λ denotes the polarization, and p is the corresponding photon wave number which need not be equal to k. The rate (probability per unit time) $\Gamma_{\rm tran}$ of an identified transition process is given by Fermi's golden rule [35],

$$\Gamma_{\rm tran} = \frac{2\pi}{\hbar}\left|M^d_{FI}\right|^2\rho, \tag{10}$$

where ρ is the density of final states.

The third-body mediated energy transfer may be represented by

$$D^\alpha + M^0 + A^0 \longrightarrow D^0 + M^0 + A^\beta.$$

Here, M denotes the nonabsorbing neighboring matter which participates in relaying energy between D and A. Two virtual photons can be created and subsequently annihilated either at the donor, third body, or acceptor with $4! = 24$ permutations. Therefore, the quantum amplitude for "indirect" coupling M^i_{FI} is calculated from the fourth term in the time-dependent perturbation series explicitly given as follows, with the superscript i on the left denoting "indirect":

$$M^i_{FI} = \sum_{R,S,T}\frac{\langle F|H_{\rm int}|T\rangle\langle T|H_{\rm int}|S\rangle\langle S|H_{\rm int}|R\rangle\langle R|H_{\rm int}|I\rangle}{(E_I - E_R)(E_I - E_S)(E_I - E_T)}. \tag{11}$$

The total matrix element is given by the sum of direct and indirect terms in Eqs. (4) and (11), and the transfer rate is then seen to be a sum of three terms, namely,

$$\begin{aligned}\Gamma^{\rm total}_{\rm tran} &= \frac{2\pi}{\hbar}\left|M^d_{FI} + M^i_{FI}\right|^2\rho \\ &= \frac{2\pi}{\hbar}\left[\left|M^d_{FI}\right|^2 + \left|M^i_{FI}\right|^2 + 2\,{\rm Re}\,\overline{M}^d_{FI}M^i_{FI}\right]\rho \\ &= \Gamma^d_{\rm tran} + \Gamma^i_{\rm tran} + \Gamma^{\rm int}_{\rm tran},\end{aligned} \tag{12}$$

where the first term of Eq. (12) was given by Eq. (10), and the third term is a quantum interference contribution to the rate arising from both direct and indirect mechanisms.

Further, the space around the donor can be divided into four zones: the Dexter zone, near-field zone, intermediate zone, and far zone [36]. Therefore, it is worth observing that other forms of coupling are also possible. Over distances of ~1 nm or less, donor-acceptor energy transfer is mediated by an electron exchange involving wave-function overlap (the ideal dipole approximation breaks in this region); this mechanism was first formulated by Dexter to account for the phenomenon of sensitized luminescence [37].

III. DIRECT ENERGY TRANSFER

For the case of direct energy transfer, electronic energy transfer from a donor to an acceptor in the absence of a surrounding medium is depicted in Fig. 2 and described by the Hamiltonian in Eq. (1) when $\xi = D, A$. The quantum

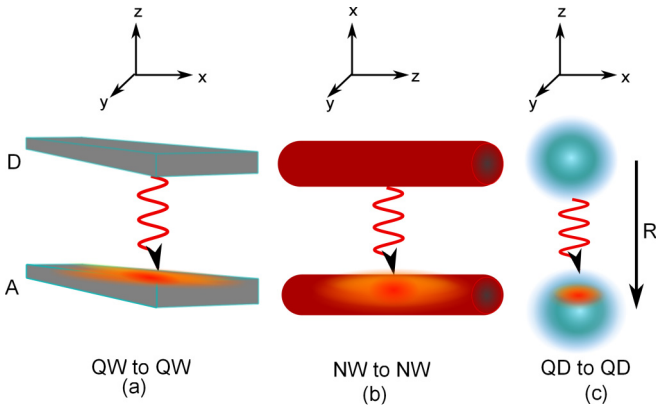

FIG. 2. (Color online) Schematics for the direct resonance energy transfer of (a) QW to QW (b) NW to NW, and (c) QD to QD.

amplitude can be calculated from Eq. (4),

$$\begin{aligned}\left\langle R^1_1|H_{\rm int}|I\right\rangle &= \langle 1(\mathbf{p},\lambda); D^0A^0| - \boldsymbol{\mu}(D)\cdot\boldsymbol{E_m}(\boldsymbol{R}_D) \\ &\quad -\boldsymbol{\mu}(A)\cdot\boldsymbol{E_m}(\boldsymbol{R}_A)|D^\alpha A^0;0\rangle \\ &= i\sum_m\left(\frac{\hbar cp}{2V\epsilon_0}\right)^{1/2}\mu^{0\alpha}_i(D)E^*_{mi}(\boldsymbol{R}_D).\end{aligned} \tag{13}$$

Here, $m = \{\boldsymbol{p},\lambda\}$ represents the photonic modes, V is an arbitrary quantization volume, and i, j are Cartesian coordinates:

$$\left\langle F|H_{\rm int}|R^1_1\right\rangle = -i\sum_m\left(\frac{\hbar cp}{2V\epsilon_0}\right)^{1/2}\mu^{\beta 0}_j(A)E_{mj}(\boldsymbol{R}_A), \tag{14}$$

$$\left\langle R^2_1|H_{\rm int}|I\right\rangle = i\sum_m\left(\frac{\hbar cp}{2V\epsilon_0}\right)^{1/2}\mu^{\beta 0}_i(A)E^*_{mi}(\boldsymbol{R}_A), \tag{15}$$

$$\left\langle F|H_{\rm int}|R^2_1\right\rangle = -i\sum_m\left(\frac{\hbar cp}{2V\epsilon_0}\right)^{1/2}\mu^{0\alpha}_j(D)E_{mj}(\boldsymbol{R}_D). \tag{16}$$

The application of Eqs. (13)–(16) on (4) gives the general formula for the quantum amplitude of direct energy transfer:

$$\begin{aligned}M^d_{FI} &= \frac{\mu^{0\alpha}_i(D)\mu^{\beta 0}_j(A)}{2V\epsilon_0}\sum_m\frac{E^*_{mi}(\boldsymbol{R}_D)E_{mj}(\boldsymbol{R}_A)p}{k-p} \\ &\quad -\frac{E_{mi}(\boldsymbol{R}_D)E^*_{mj}(\boldsymbol{R}_A)p}{k+p}.\end{aligned} \tag{17}$$

In the case of direct RET, the transfer of electronic excitation may be illustrated with two Feynman diagrams. One Feynman diagram is shown in Fig. 3(a). The system's evolution through all three stages (initial, intermediate, final) via two pathways makes one object undergo a transition between states $0,\alpha,\beta$ and one photon is either created or annihilated [38].

A. Quantum well to quantum well

The one-dimensional (1D) idealization corresponds to the interaction of two parallel planar QWs. It is assumed that the dipole transition moments of the excitons are parallel and in the plane of the QWs. Therefore, the EM modes are 1D plane waves propagating in the direction z perpendicular to the QWs (only photonic modes with electric field vectors parallel to the dipole moments of excitons contribute to these

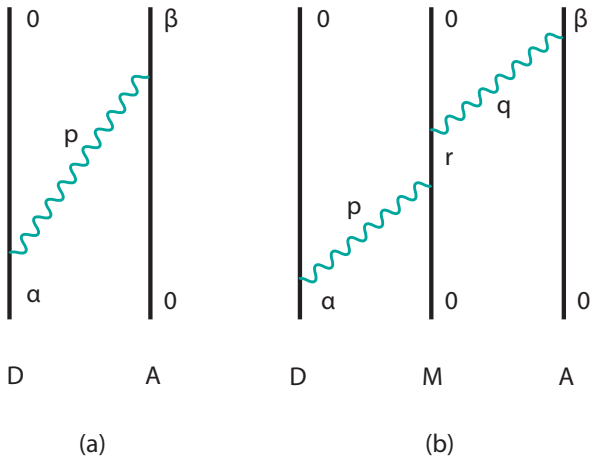

FIG. 3. (Color online) Feynman diagrams show one path of each direct and indirect RET.

calculations) [32]: $E_p(R_\xi) = e^{ip_z z_\xi}$. Directly substituting into Eq. (17) and converting the discrete summation over p_z, $\sum_{p_z} \Rightarrow \int \frac{L}{2\pi} dp_z$ to an integral yields

$$M_{FI}^d = \frac{\mu^{0\alpha}(D)\mu^{\beta 0}(A)}{4\pi A'\epsilon_0} \int_0^\infty \left(\frac{e^{ip_z R} p_z}{k - p_z} - \frac{e^{-ip_z R} p_z}{k + p_z} \right) dp_z, \tag{18}$$

where A' is area of the QW and $\boldsymbol{R} = \boldsymbol{R_A} - \boldsymbol{R_D}$.

Performing contour integration and by the residue theorem $c = p_z R$,

$$\begin{aligned} M_{FI}^d &= \frac{\mu^{0\alpha}(D)\mu^{\beta 0}(A)}{4\pi A'\epsilon_0 R} \oint_c \frac{e^{ic} kRc}{(kR - c)(kR + c)} \\ &\quad + \frac{e^{ic} c^2}{(kR - c)(kR + c)} dc \\ &= \frac{\mu^{0\alpha}(D)\mu^{\beta 0}(A)}{2A'\epsilon_0} k\{\sin(kR) - i\cos(kR)\}. \end{aligned} \tag{19}$$

The plots of Eq. (19) are shown in Figs. 4(a) and 4(d) for various values of the photon wave number corresponding to the atomic transition frequency (k) and donor-acceptor separation distance (R). In the development of the plots for Sec. III, the following values were used [39]: $|\mu^{0\alpha}(D)| = |\mu^{\beta 0}(A)| = 5 \times 10^{-30}$ C m; $\rho = 2 \times 10^{25}$ J^{-1}. Both the real and imaginary parts of the resonant dipole-dipole interaction (RDDI) oscillate with k, and the amplitude of the matrix element increases gradually according to Eq. (19), owing to the fact that the high corresponding eigenenergy ($E_{0\alpha}^D$) is analogous to the high quantum amplitude of coupling between two QWs. These dependencies of RDDI as a function of k influence the energy transfer rate to rise gradually, as illustrated in Fig. 5(a). This is because the energy transfer rate is proportional to the square modulus of the quantum amplitude of the RET process ($\Gamma_{\text{tran}} \propto |M_{FI}^d|^2$).

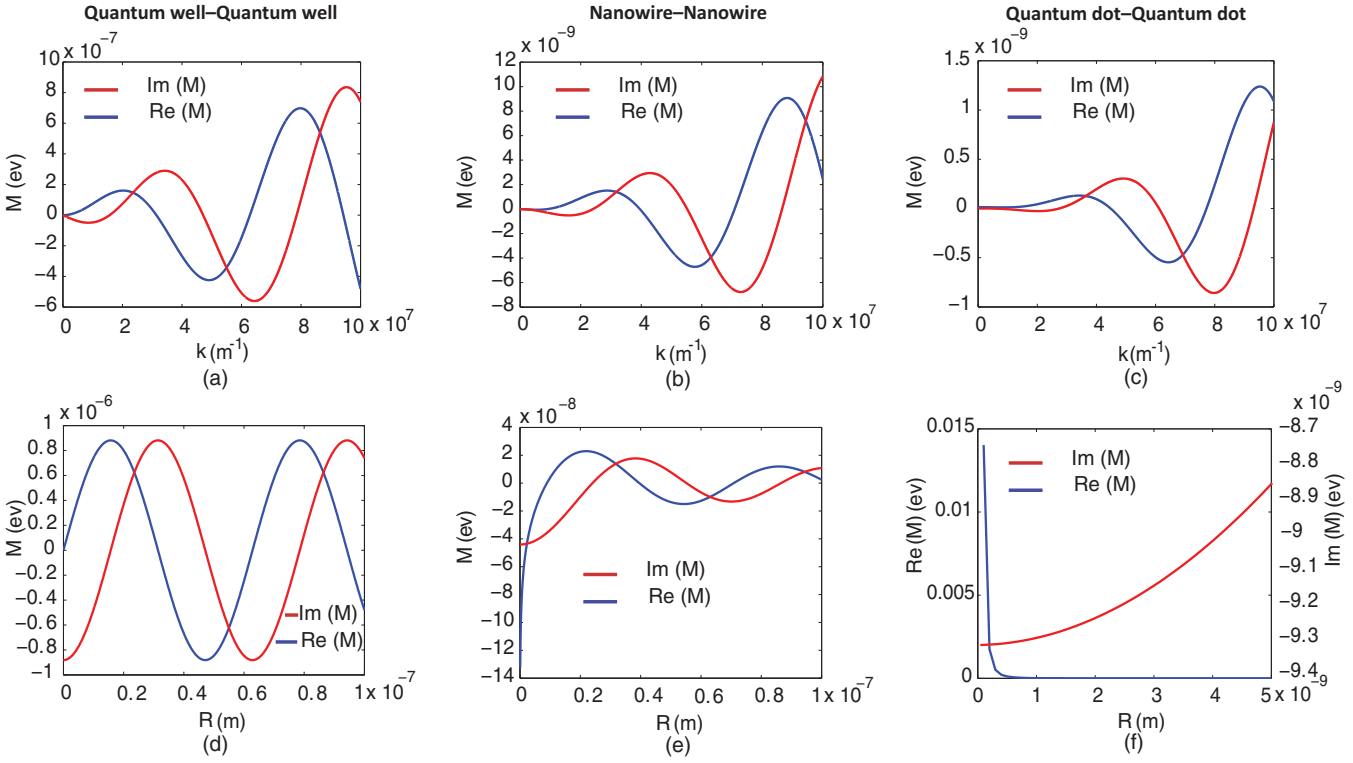

FIG. 4. (Color online) Direct RET: RDDI strengths in 1D, 2D, and 3D free-space environments are shown in (a)–(c), respectively, as a function of the wave number corresponding to the resonant atomic transition frequency. (d)–(f) show RDDI as a function of the relative distance between D and A. In each panel, the blue solid line represents the real part of the RDDI while the red solid line shows the imaginary part of the RDDI.

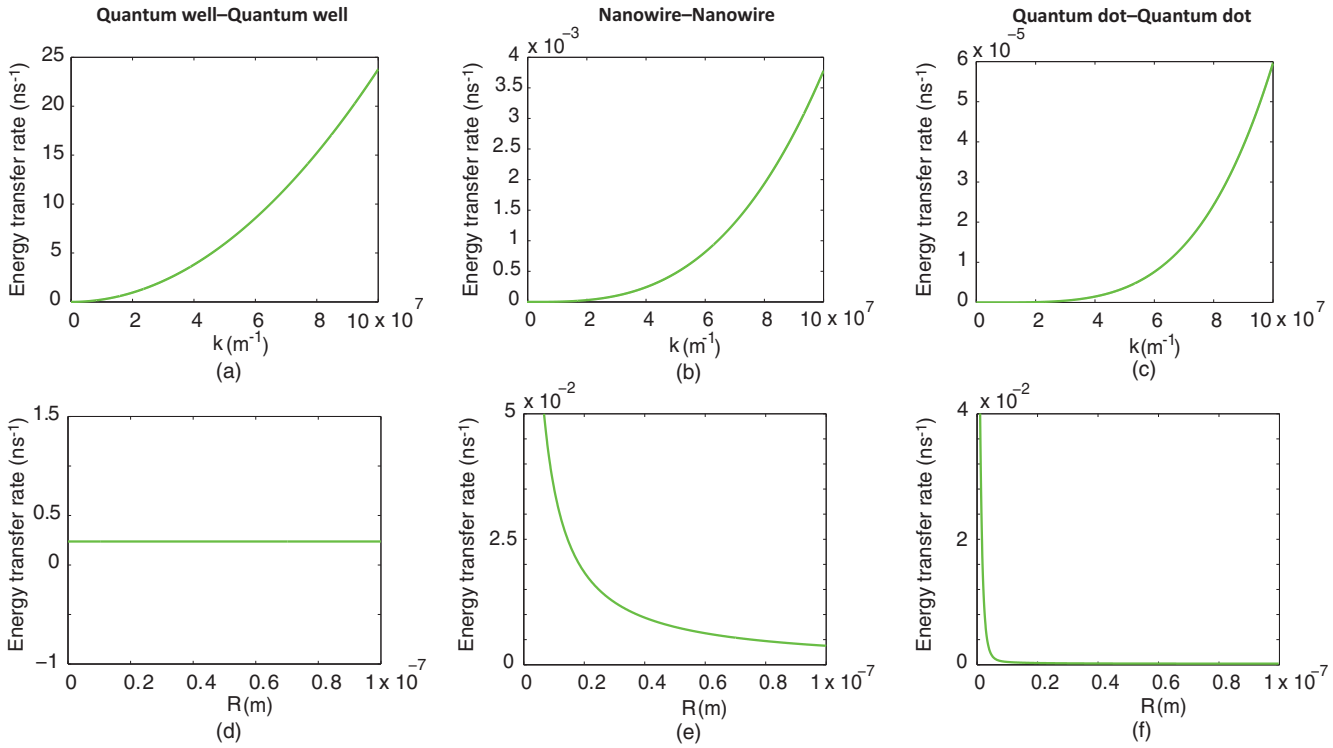

FIG. 5. (Color online) Direct RET: Energy transfer rates in 1D, 2D, and 3D free-space environments are shown in (a)–(c), respectively, as a function of the wave number corresponding to the resonant atomic transition frequency. (d)–(f) show the transfer rate as a function of the relative distance between D and A. The distance invariance exhibited in (d) signifies lossless unidirectional transfer (see the discussion in text).

Substitution of Eq. (19) into the Fermi's golden rule expression yields

$$\Gamma^{d}_{\text{tran}} = \frac{\pi |\mu^{0\alpha}(D)|^2 |\mu^{\beta 0}(A)|^2 k^2}{2\hbar (A'\epsilon_0)^2}\rho. \tag{20}$$

Imposing an effective limitation on the direction of virtual photon propagation has an element of correlation with the physics of energy transfer along a waveguide (in principle, there are no physical losses in such a system, since we assume the transmission medium is dispersion free). Therefore, both the real and imaginary parts of the RDDI vary between the same minimum and maximum quantum amplitudes, resulting in a constant energy transfer rate, as sketched in Fig. 5(d).

B. Nanowire to nanowire

Idealized two-dimensional (2D) parallel nanowires of length L separated by a distance R are considered. EM waves are modeled using the Hankel function of order n [40], $E_p(R_\xi) = \sum_n H_n(pR_\xi)e^{in\alpha}$, where R and α are the radial and angular coordinates, respectively. Directly substituting into Eq. (17) and converting the discrete summation over the virtual photon wave vector yields

$$M^{d}_{FI} = \frac{\mu^{0\alpha}(D)\mu^{\beta 0}(A)}{8\pi^2 L\epsilon_0}\int_0^{\infty}\int_0^{2\pi}\left(\frac{H_0(pR)p^2}{k-p} - \frac{H_0^*(pR)p^2}{k+p}\right)d\phi dp. \tag{21}$$

Expanding the Hankel function, performing contour integration, and by the residue theorem,

$$M^{d}_{FI} = \frac{\mu^{0\alpha}(D)\mu^{\beta 0}(A)}{2\pi L R^2\epsilon_0}\oint_c \frac{ic^2kRY_0(c) + c^3J_0(kR)}{(kR-c)(kR+c)}dc = \frac{\mu^{0\alpha}(D)\mu^{\beta 0}(A)k^2}{4L\epsilon_0}\{Y_0(kR) - iJ_0(kR)\}. \tag{22}$$

The energy transfer rate can be obtain from Eq. (10),

$$\Gamma^{d}_{\text{tran}} = \frac{\pi |\mu^{0\alpha}(D)|^2 |\mu^{\beta 0}(A)|^2 k^4}{8L^2\epsilon_0{}^2\hbar}\left\{Y_0^2(kR) + J_0^2(kR)\right\}\rho. \tag{23}$$

Figures 4(b) and 5(b) illustrate the functional dependence of RDDI against k and R. The ensuing results are of a form similar to the QW case, with the quantum amplitude and the energy transfer efficiency increasing with wave number (higher resonant frequencies $\omega_{\alpha 0}$ furnish higher RDDIs compared to lower resonant frequencies). It is observed that due to the behavior of the virtual photon propagation in a 2D realm, the real and imaginary parts of RDDI decrease with R by following the second and first kind of Bessel functions, respectively [see Fig. 4(e)]. This can be understood from the derivation of Eq. (22), resulting in a gradual decline of the energy transfer efficiency with distance, as shown in Fig. 5(e). The energy transfer efficiency in the donor-acceptor separation distance from 1 to 15 nm exhibits a higher distance dependence than the transfer rate beyond 15 nm. This is analogous to the analysis done in Ref. [25] (with a log-log plot of the transfer function against distance R), and unified theory [26]. Nevertheless, our results for NWs deliver a general distance dependence for the near zone and far zone which is proportional to

$Y_0^2(kR) + J_0^2(kR)$, excluding the Dexter zone, which is more prominent within the range of wave-function overlap.

C. Quantum dot to quantum dot

In the three dimensional (3D) realm, a pair of QDs separated by distance R is considered: $E_m(R_\xi) = \boldsymbol{e}^{(\lambda)}(\boldsymbol{p})e^{i\boldsymbol{p}\cdot\boldsymbol{R}}$. Direct substitution into Eq. (17) and converting the discrete summation over virtual photon wave vector gives

$$M_{FI}^d = \frac{\mu_i^{0\alpha}(D)\mu_j^{\beta 0}(A)}{2\epsilon_0}\int_0^\infty\int_0^{2\pi}\int_{-1}^{1}\left[\boldsymbol{e}_i^{(\lambda)}(\boldsymbol{p})\overline{\boldsymbol{e}}_j^{(\lambda)}(\boldsymbol{p})\right] \times\left\{\frac{e^{i\boldsymbol{p}\cdot\boldsymbol{R}}p^3}{k-p} - \frac{e^{-i\boldsymbol{p}\cdot\boldsymbol{R}}p^3}{k+p}\right\}d(\cos\theta)d\phi dp, \quad (24)$$

where $\boldsymbol{e}^{(\lambda)}(\boldsymbol{p})$ is the polarization vector,

$$M_{FI}^d = \mu_i^{0\alpha}(D)V_{ij}(k,\boldsymbol{R})\mu_j^{\beta 0}(A). \quad (25)$$

The coupling tensor V_{ij} is given by

$$\begin{aligned}V_{ij}(k,\boldsymbol{R}) = \frac{1}{4\pi\epsilon_0 R^3}&\{(\delta_{ij} - 3\hat{R}_i\hat{R}_j)[\cos(kR) + kR\sin(kR)]\\ &-(\delta_{ij} - \hat{R}_i\hat{R}_j)[k^2R^2\cos(kR)]\}\\ &-i\{(\delta_{ij} - 3\hat{R}_i\hat{R}_j)[\sin(kR) - kR\cos(kR)]\\ &-(\delta_{ij} - \hat{R}_i\hat{R}_j)[k^2R^2\sin(kR)]\}. \quad (26)\end{aligned}$$

The energy transfer rate between two QDs can be expressed as

$$\Gamma_{\text{tran}}^d = \frac{2\pi}{\hbar}|\mu^{0\alpha}(D)|^2|\mu^{\beta 0}(A)|^2V_{ij}(k,\boldsymbol{R})\overline{V}_{ij}(k,\boldsymbol{R})\rho. \quad (27)$$

This work is similar to the numerous studies reported for molecules discussed in Refs. [26,41] and previously studied for QDs in Ref. [42]. In the small separation distances ($kR \ll 1$), the imaginary part of the probability amplitude is negligibly small compared to that of the real part, as depicted in Fig. 4(f). Therefore, the energy transfer rate decreases with respect to R, as illustrated in Fig. 5(f). In the near-zone limit, when QDs are separated by a distance significantly less than k^{-1}, though necessarily beyond a significant wave-function overlap, the interaction strength declines with distance. This is the well-known inverse sixth-power distance dependence discovered in the unified theory [26,42]. The variations of the quantum amplitude and the energy transfer rate as a function of wave number depicted in Figs. 4(c) and 5(c) bear the same explanations as above (see Secs. III A and III B). In the context of unified theory, the initial and final terms of the real and imaginary parts of Eq. (26) effectively signify an electromagnetic mediator of completely "virtual" and "real" characteristics, respectively [26]. Therefore, it is ascertained that the first term in each real and imaginary part dominates in the short range ($kR \ll 1$), and the last term in the long range ($kR \gg 1$), leading to R^{-6} and R^{-2} distance dependencies.

IV. INDIRECT ENERGY TRANSFER

Let us now introduce a third quantum object, M, which has the same dimensionality as D and A, as shown in Fig. 6. M has the capacity to act as a bridge species between D and A, relaying the energy from the donor to acceptor, but otherwise remaining unchanged. Its positioning directly between D and A may be assumed to preclude direct coupling between the donor and acceptor. The exchange of an additional virtual photon q with a passive M is the lowest-order coupling process that elevates RET to a third-body mediated RET. Therefore, the fourth-order perturbation theory forms the basis for identifying passive third-body effects on RET, which is stated in Eq. (11).

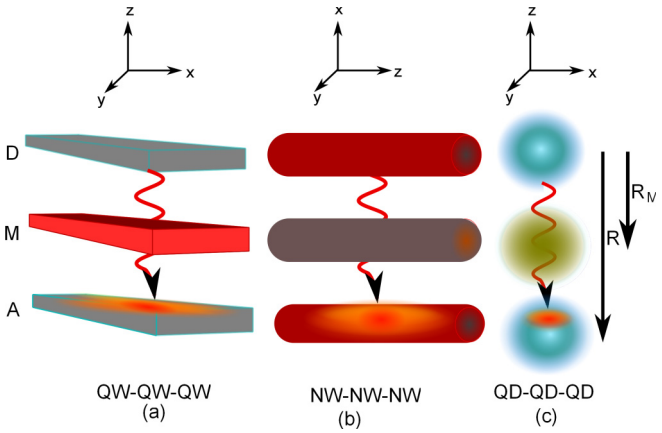

FIG. 6. (Color online) Schematics for the third-body modified resonance energy transfer of (a) QW to QW, (b) NW to NW, and (c) QD to QD. R is the distance between D and A, and R_M is the distance between D and M.

The four transition events (W, X, Y, Z) cause five stages of the system's evolution, labeled I, R, S, T, F in chronological order. Each stage is associated with various possible states of the overall system. Therefore, 24 Feynman graphs contribute to the quantum amplitude. One such Feynman diagram is shown in Fig. 3(b) for illustrative purposes. Figure 7 illustrates the system's evolution through all five stages with one state-sequence diagram. Each of the 24 pathways through the state-sequence network represents one Feynman diagram [22]. For example, consider one pathway, $W \to X \to Y \to Z$, to obtain the matrix element. When $\xi = D, M, A$ at each event, one object undergoes a transition between states $0, \alpha, r, \beta$ and one photon is either created or annihilated:

$$\langle R|H_{\text{int}}|I\rangle = i\sum_m\left(\frac{\hbar cp}{2V\epsilon_0}\right)^{1/2}\mu_i^{0\alpha}(D)E_{mi}^*(\boldsymbol{R}_D), \quad (28)$$

$$\langle S|H_{\text{int}}|R\rangle = -i\sum_m\left(\frac{\hbar cp}{2V\epsilon_0}\right)^{1/2}\mu_k^{r0}(M)E_{mk}(\boldsymbol{R}_M), \quad (29)$$

$$\langle T|H_{\text{int}}|S\rangle = i\sum_n\left(\frac{\hbar cq}{2V\epsilon_0}\right)^{1/2}\mu_l^{0r}(M)E_{nl}^*(\boldsymbol{R}_M), \quad (30)$$

$$\langle T|H_{\text{int}}|S\rangle = -i\sum_n\left(\frac{\hbar cq}{2V\epsilon_0}\right)^{1/2}\mu_j^{\beta 0}(A)E_{nj}(\boldsymbol{R}_A). \quad (31)$$

Here, $m = \{\boldsymbol{p},\lambda\}$ and $n = \{\boldsymbol{q},\lambda'\}$ represent the photonic modes, where $\boldsymbol{p},\boldsymbol{q}$ are wave vectors and λ,λ' denote the

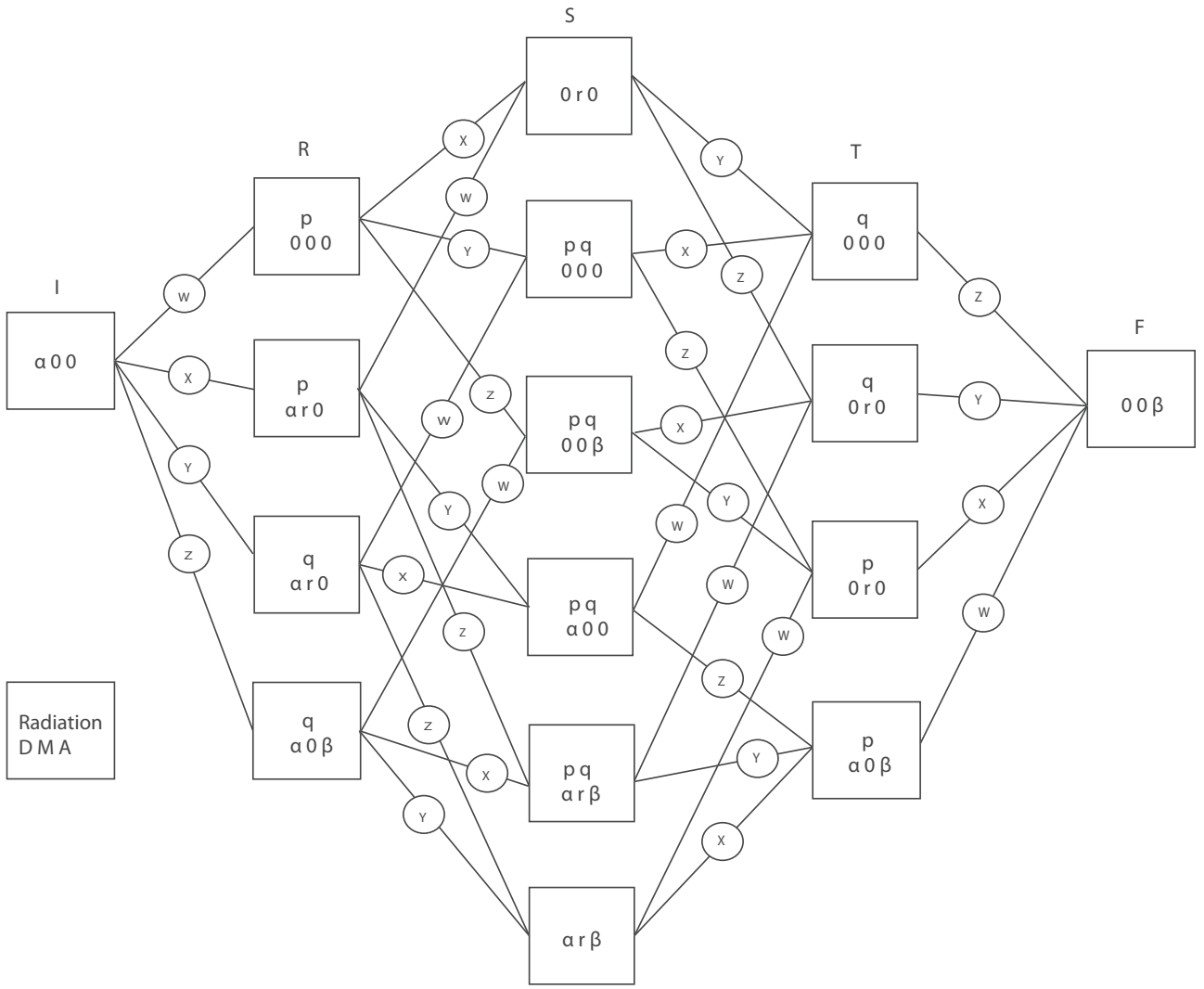

FIG. 7. State-sequence diagram for the third-body modified RET. Time progresses left to right, with each of the 16 boxes representing one of the possible overall states of the system in one of the five stages I, R, S, T, F. Each overall state comprises states for each changing sub-system—the radiation (p,q denote virtual photons), and D, M, A.

polarization. The sum over all 24 event orderings yields

$$M^i_{FI} = -\sum_m \sum_n \left(\frac{\hbar c p}{2V\epsilon_0}\right)\left(\frac{\hbar c q}{2V\epsilon_0}\right)\mu_i^{0\alpha}(D)\mu_j^{\beta 0}(A)\alpha_{kl}(M;k)$$
$$\times\left\{\frac{E_{mi}(\boldsymbol{R}_D)E^*_{mk}(\boldsymbol{R}_M)E_{nj}(\boldsymbol{R}_A)E^*_{nl}(\boldsymbol{R}_M)}{(p-k)(q-k)} + \frac{E_{mi}(\boldsymbol{R}_D)E^*_{mk}(\boldsymbol{R}_M)E^*_{nj}(\boldsymbol{R}_A)E_{nl}(\boldsymbol{R}_M)}{(p-k)(q+k)}\right.$$
$$\left. + \frac{E^*_{mi}(\boldsymbol{R}_D)E_{mk}(\boldsymbol{R}_M)E_{nj}(\boldsymbol{R}_A)E^*_{nl}(\boldsymbol{R}_M)}{(p+k)(q-k)} + \frac{E^*_{mi}(\boldsymbol{R}_D)E_{mk}(\boldsymbol{R}_M)E^*_{nj}(\boldsymbol{R}_A)E_{nl}(\boldsymbol{R}_M)}{(p+k)(q+k)}\right\}, \tag{32}$$

$$\alpha_{kl}(M;k) = \sum_r \mu_k^{r0}(M)\mu_l^{0r}(M)\left\{\frac{1}{E_{r0}-\hbar c k} + \frac{1}{E_{r0}+\hbar c k}\right\}. \tag{33}$$

Here, $\alpha_{kl}(M;k)$ is the dynamic polarizability of particle M [43,44].

Consider $\boldsymbol{R}' = \boldsymbol{R}_M - \boldsymbol{R}_D$ and $\boldsymbol{R}'' = \boldsymbol{R}_A - \boldsymbol{R}_M$, so that $\boldsymbol{R} = \boldsymbol{R}_A - \boldsymbol{R}_D$ for the next calculations.

A. Quantum well to quantum well in the vicinity of another quantum well

We introduce another planer QW between the two QWs described in Sec. III A. Direct substitution into Eq. (32)

yields

$$M_{FI}^{i} = -\frac{\mu_i^{0\alpha}(D)\mu_j^{\beta 0}(A)}{(2V\epsilon_0)^2}\sum_{\boldsymbol{p}}\sum_{\boldsymbol{q}}\alpha_{kl}(M;k)p_z q_z\left\{\frac{e^{-ip_z z'}e^{iq_z z''}}{(p-k)(q-k)}+\frac{e^{-ip_z z'}e^{-iq_z z''}}{(p-k)(q+k)}+\frac{e^{ip_z z'}e^{iq_z z''}}{(p+k)(q-k)}+\frac{e^{ip_z z'}e^{-iq_z z''}}{(p+k)(q+k)}\right\}, \tag{34}$$

$$M_{FI}^{i} = -\frac{\mu_i^{0\alpha}(D)\mu_j^{\beta 0}(A)}{(2V\epsilon_0)^2}\sum_{\boldsymbol{p}}\sum_{\boldsymbol{q}}\alpha_{kl}(M;k)p_z q_z\left(\frac{e^{-ip_z z'}}{p-k}+\frac{e^{ip_z z'}}{p+k}\right)\left(\frac{e^{iq_z z''}}{q-k}+\frac{e^{-iq_z z''}}{q+k}\right). \tag{35}$$

Converting the discrete summation over p_z,q_z to an integral yields

$$M_{FI}^{i} = -\frac{\mu_i^{0\alpha}(D)\mu_j^{\beta 0}(A)}{(2A'\epsilon_0)^2}\int_0^\infty\int_0^\infty\alpha_{kl}(M;k)p_z q_z\left(\frac{e^{-ip_z z'}}{p-k}+\frac{e^{ip_z z'}}{p+k}\right)\left(\frac{e^{iq_z z''}}{q-k}+\frac{e^{-iq_z z''}}{q+k}\right)dq_z dp_z. \tag{36}$$

In a manner similar to the previous case in Sec. III, the quantum amplitude, performing contour integration, and using the residue theorem twice over two virtual photons becomes

$$M_{FI}^{i} = \frac{\mu_i^{0\alpha}(D)\mu_j^{\beta 0}(A)k^2}{(2A'\epsilon_0)^2}\alpha_{kl}(M;k)e^{ikR}. \tag{37}$$

This is independent of the relative positioning of the third QW between D and A. The application of the Fermi's golden rule gives rise to the following expression for the transfer rate:

$$\Gamma_{\text{tran}}^{i} = \frac{\pi|\mu^{0\alpha}(D)|^2|\mu^{\beta 0}(A)|^2k^4}{8\hbar(A'\epsilon_0)^4}\alpha_{kl}(M;k)\overline{\alpha}_{kl}(M;k). \tag{38}$$

In the development of the plots in Sec. IV, the following values were used [39]: $|\mu^{0\alpha}(D)| = |\mu^{\beta 0}(A)| = 5\times 10^{-30}$ C m; $\rho = 2\times 10^{25}$ J^{-1}. $\alpha_{kl}(M;k)$ is the ground state dynamic polarizability of the third nanostructure M at the resonant frequency $\omega_{0\alpha} = ck$. Polarizability values are related to the refractive index by the Clausius-Mossotti equation, and an in-depth analysis was carried out in Refs. [31,43,44]. Therefore, in the development of the graphs, we assume $|\alpha_{kl}(M;k)|$ of the included intermediary takes a typical value of 8×10^{-40} J^{-1} C^2 m^2. The plots of Eq. (37) are shown in Figs. 8(a) and 8(d) for various values of k and R. These figures exhibit similar patterns to those observed for direct energy transfer. Nevertheless, the quantum amplitude is lower than that of a direct interaction due to four light-matter interactions which arise from the interference of the third QW [Eq. (36)]. This effect can be observed in the corresponding energy transfer rate depicted in Fig. 9(a). Similar to the direct interaction, RDDI oscillates at a constant amplitude with respect to distance (R) in a dispersion-free medium. Therefore, the RDDI and the energy transfer rate do not depend on the position of the third QW [see Figs. 8(d) and 9(d)].

B. Nanowire to nanowire in the vicinity of another nanowire

In a similar manner as to the previous case, we introduce another 2D idealized NW between the two NWs described in Sec. III B. Direct substitution into Eq. (32) and converting the discrete summation over wave vectors $\boldsymbol{p}$ and $\boldsymbol{q}$ yields

$$\begin{aligned}M_{FI}^{i} = -\frac{\mu_i^{0\alpha}(D)\mu_j^{\beta 0}(A)}{(2L\epsilon_0)^2}&\int_0^\infty\int_0^{2\pi}\int_0^\infty\int_0^{2\pi}\alpha_{kl}(M;k)p^2q^2\\&\times\left(\frac{H_0^*(pR')}{p-k}+\frac{H_0(pR')}{p+k}\right)\\&\times\left(\frac{H_0(qR'')}{q-k}+\frac{H_0^*(qR'')}{q+k}\right)dq\,d\phi\,dp\,d\varphi.\end{aligned} \tag{39}$$

Performing a contour integration and using the residue theorem with respect to the properties of the two virtual photons, the above expression becomes

$$\begin{aligned}M_{FI}^{i} = -\frac{\mu_i^{0\alpha}(D)\mu_j^{\beta 0}(A)k^4}{16(L\epsilon_0)^2}&\alpha_{kl}(M;k)\\&\times\{[Y_0(kR')Y_0(kR'')-J_0(kR')J_0(kR'')]\\&-i[Y_0(kR')J_0(kR'')+J_0(kR')Y_0(kR'')]\}.\end{aligned} \tag{40}$$

Therefore, the energy transfer rate becomes

$$\begin{aligned}\Gamma_{\text{tran}}^{i} = \frac{\pi|\mu^{0\alpha}(D)|^2|\mu^{\beta 0}(A)|^2k^8}{128(L\epsilon_0)^4\hbar}&\alpha_{kl}(M;k)\overline{\alpha}_{kl}(M;k)\\&\times\{[Y_0(kR')Y_0(kR'')-J_0(kR')J_0(kR'')]^2\\&+[Y_0(kR')J_0(kR'')+J_0(kR')Y_0(kR'')]^2\}\rho.\end{aligned} \tag{41}$$

Figure 8(b) illustrates the variation of the matrix element as a function of the photon wave number (k) expressed in Eq. (40). Similar to the previous sections, the quantum amplitude increases with the wave number, leading to a gradual increase in the energy transfer rate depicted in Fig. 9(b). In the presence of a neighboring mediator, the matrix element for the mechanism of RET is duly modified to Eq. (41). Compared to the direct interaction of two nanowires in Eq. (22), the creation and annihilation of two virtual photons reduce the quantum amplitude of the indirect interaction as a function of the separation distance (R). Therefore, as illustrated in Figs. 8(e) and 9(e), the influence of the included intermediary nanowire (M) becomes more prominent and almost constant in the range of 20–80 nm of the donor-acceptor separation distance. These effects of neighboring components, not specifically absorbing in the same wavelength region as the excitation donor or acceptor, can be understood in terms of their electronic

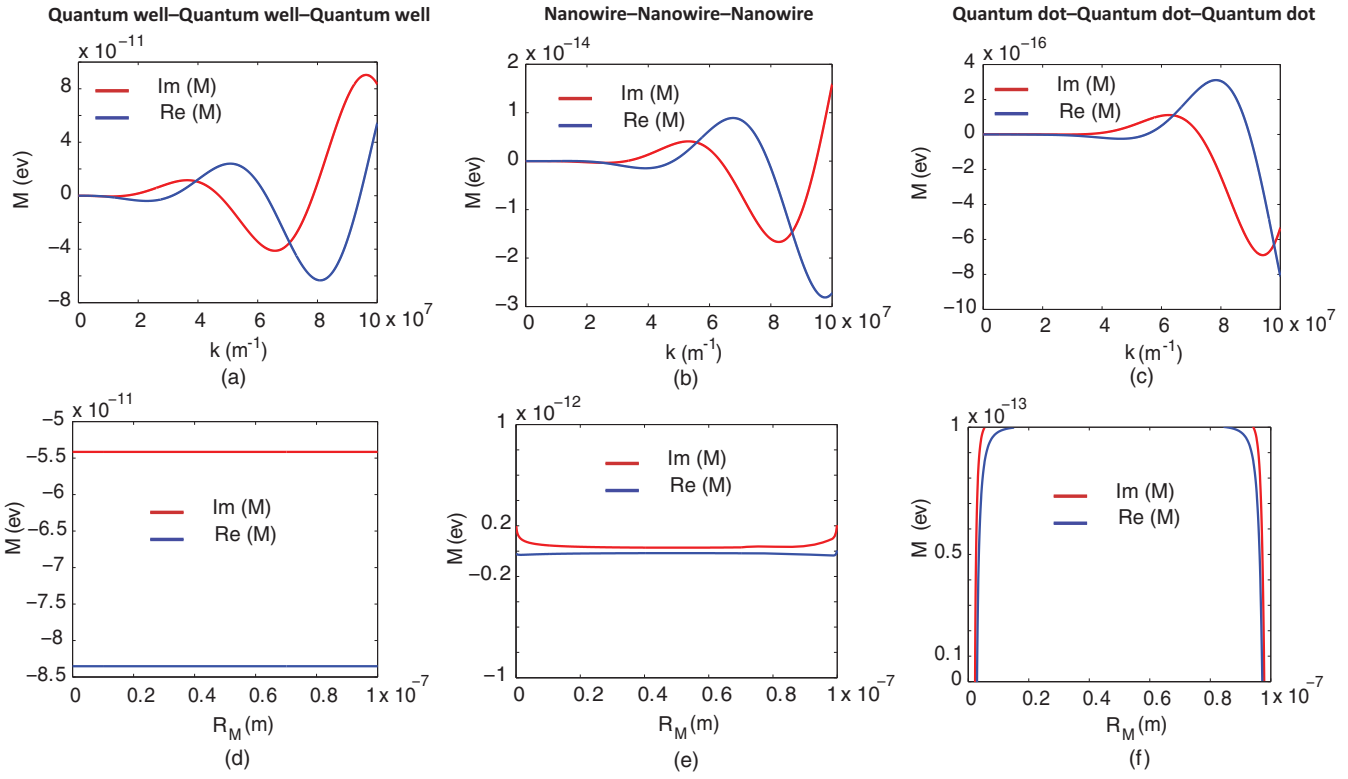

FIG. 8. (Color online) Indirect RET: RDDI strengths in 1D, 2D, and 3D free-space environments are shown in (a)–(c), respectively, as a function of the wave number corresponding to the resonant atomic transition frequency. (d)–(f) show RDDI as a function of the relative distance between D and M. In each panel, the blue solid line represents the real part of the RDDI while the red solid line shows the imaginary part of the RDDI.

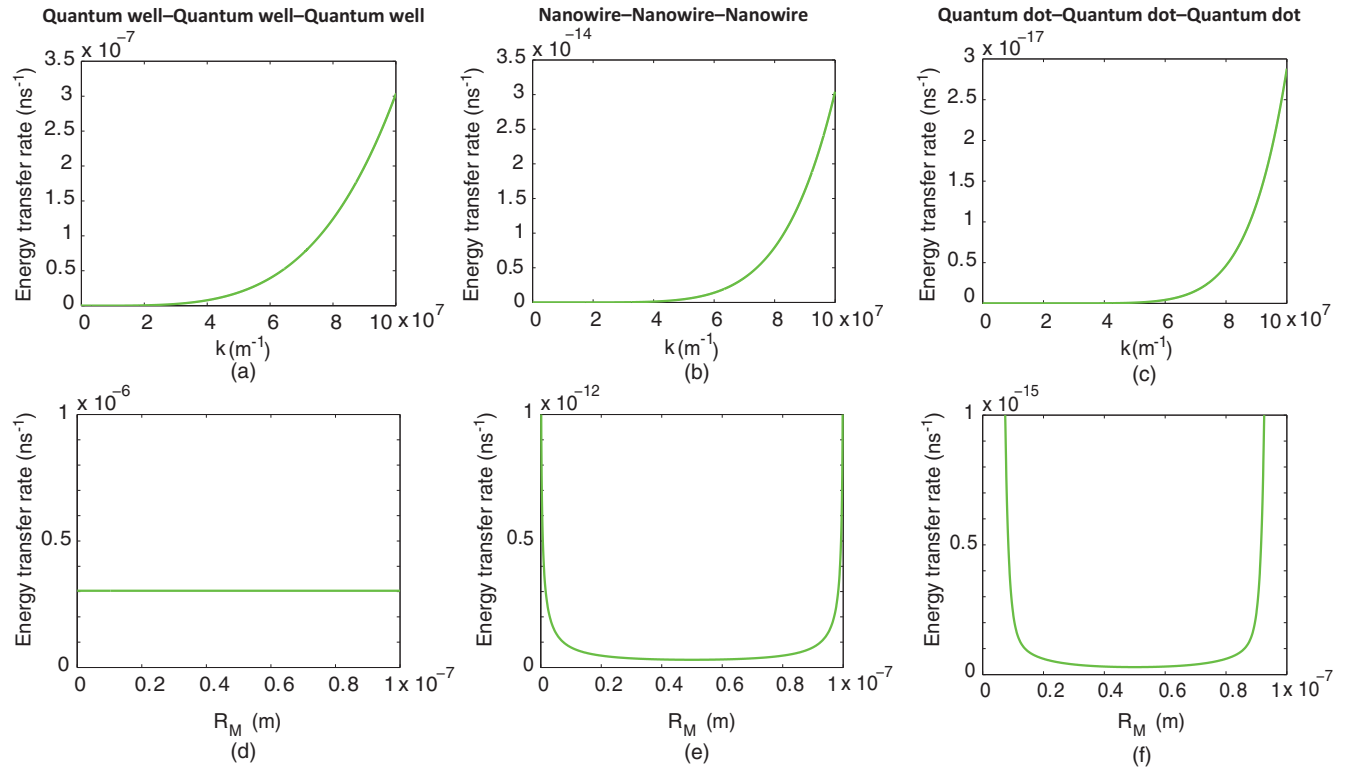

FIG. 9. (Color online) Indirect RET: Energy transfer rates in 1D, 2D, and 3D free-space environments are shown in (a)–(c), respectively, as a function of the wave number corresponding to the resonant atomic transition frequency. (d)–(f) show the transfer rate as a function of the relative distance between D and M.

polarizability $[\alpha_{kl}(M;k)]$ [31]. For values of $R', R'' < 1$ nm that generally signify the possibility of wave-function overlap (the Dexter zone where electron exchange would occur), the expressions presented above are less meaningful as the third body could no longer be regarded as an electronically separate chemical entity, and in recognition of this, the values of the matrix element and energy transfer rate in this region should not be regarded as physically significant.

C. Quantum dot to quantum dot in the vicinity of another quantum dot

Another QD is inserted between the acceptor-donor QD pair. Direct substitution into Eq. (32) and converting the discrete summation over wave vectors $\boldsymbol{p}$ and $\boldsymbol{q}$ yields

$$M_{FI}^{i} = -\frac{\mu_i^{0\alpha}(D)\mu_j^{\beta 0}(A)}{(2\epsilon_0)^2}\int_0^{\infty}\int_0^{2\pi}\int_{-1}^{1}\int_0^{\infty}\int_0^{2\pi}\int_{-1}^{1} \times \boldsymbol{e}_i^{(\lambda)}(\boldsymbol{p})\overline{\boldsymbol{e}}_l^{(\lambda)}(\boldsymbol{p})\boldsymbol{e}_j^{(\lambda)}(\boldsymbol{q})\overline{\boldsymbol{e}}_k^{(\lambda)}(\boldsymbol{q})\alpha_{kl}(M;k)p^3q^3 \times\left(\frac{e^{-i\boldsymbol{p}\cdot\boldsymbol{R}'}}{p-k}+\frac{e^{i\boldsymbol{p}\cdot\boldsymbol{R}'}}{p+k}\right)\left(\frac{e^{i\boldsymbol{q}\cdot\boldsymbol{R}''}}{q-k}+\frac{e^{-i\boldsymbol{q}\cdot\boldsymbol{R}''}}{q+k}\right) \times d(\cos\theta)d\phi dq dq d(\cos\vartheta)d\varphi dp. \quad (42)$$

Similar to Sec. III, the quantum amplitude, performing contour integration, and implementing the residue theorem over both virtual photons results in

$$M_{FI}^{i} = -\mu_i^{0\alpha}(D)\mu_j^{\beta 0}(A)\alpha_{kl}(M;k)V_{il}(k,\boldsymbol{R}')V_{kj}(k,\boldsymbol{R}''). \quad (43)$$

The application of the Fermi's golden rule leads to the following expression for the transfer rate:

$$\Gamma_{\text{tran}}^{i} = \frac{2\pi\rho}{\hbar}|\mu^{0\alpha}(D)|^2|\mu^{\beta 0}(A)|^2|\alpha_{kl}(M;k)|^2 \times V_{il}(k,\boldsymbol{R}')\overline{V}_{il}(k,\boldsymbol{R}')V_{kj}(k,\boldsymbol{R}'')\overline{V}_{kj}(k,\boldsymbol{R}''). \quad (44)$$

This is similar to the numerous studies reported for molecules discussed in Refs. [31,39], with one important difference. Due to the geometric placement and the physical nature of the components in the present calculation, the inclusion of component M here signifies that the direct transfer of energy from D to A is no longer contributing to the overall quantum amplitude. In a similar manner as discussed above, from Eq. (43), it is observed that the indirect RDDI is lower than the direct RDDI due to four matter-radiation interactions which arise from the influence of the third QD. This impacts on the indirect energy transfer efficiency, consistent with Fermi's golden rule, which can be observed in Figs. 8(c) and 9(c). In addition, the transfer of electronic excitation via two virtual photons yields RDDI and the energy transfer rate to vary with the relative distance R_M, as shown in Figs. 8(f) and 9(f). In the near-zone limit, the indirect transfer rate is proportional to $(R')^{-6}(R'')^{-6}$. On the other hand, in the long range, applying limits of $kR' \gg 1$ and $kR'' \gg 1$ yields $(R')^{-2}(R'')^{-2}$ distance dependence.

V. DISCUSSION

In Sec. III the direct energy transfer rates and corresponding quantum amplitudes for different nanostructures have been derived and the results are discussed with figures. The results have demonstrated the dimensionality of the nanostructure along with the variation of EM modes determining the controllability of the resonance energy transfer rate.

The influence of a nonabsorbing neighboring matter of the same dimensionality on RET efficiency has been studied in Sec. IV. Figures 8(a)–8(c) show the variation of RDDI with the photon wave number corresponding to the atomic transition frequency, exhibiting patterns similar to the ones observed for direct energy transfer. In the QW case, both Re(RDDI) and Im(RDDI) do not vary with the R_M due to the unidirectional characteristics of the virtual photons in 1D nanostructures. In passing, we note the much greater complexity that ensues upon removal of the directional constraint on the coupling photon. To this end, we identified a potential alternative method in terms of essentially discretized transition moment elements. In that case, each virtual photon trajectory is represented as part of a conical surface at an arbitrary angle to the normal to the donor and acceptor planes. However, such an analysis proves unfruitful, in terms of delivering suitably analytic results; this represents a scope for further development of the theory.

Exploration of the quantum amplitude is the core contribution of all derivations. Our calculations for quantum amplitude are based on the Schrödinger state vector representation of quantum dynamics, where the matrix element for RET is represented as a sum of differently time-ordered contributions [20]. However, one can apply alternative formulations, for example, in terms of a density matrix in Liouville space [45]. Furthermore, the coupling between nanostructures of mixed dimensionality involves discovering the suitable quantization volume in each case (i.e., QW to QD). Moreover, the quantum interference is an interesting quantity which, together with the direct and indirect transfer rates, determines the total energy transfer (the interference contribution to the total energy transfer rate for molecules is discussed in Refs. [30,31]). Thus, the coupling between nanostructures of mixed dimensionality and the quantum interference for the direct and indirect energy transfer of nanostructures signify prospective future developments of the current research.

VI. CONCLUSIONS

In this paper, the direct RET between two nanostructures and the influence of a third quantum object has been studied using the theory of molecular quantum electrodynamics. We envisioned six cases, 1D, 2D, and 3D for QW, NW, and QD, respectively, as well as the influence of an included intermediary in each case. The quantum amplitude and rate equations are derived for all the cases.

The results have demonstrated the intricate interplay of the relative distance, atomic transition frequency, dimensionality of the object, and the effect of the neighboring matter in determining the efficiency of the energy transfer. Although the Förster theory is very well suited to many situations, the distance dependence and mediation of EET coupling are more complicated than the traditional Förster theory predicts. The origin of these complications is deeply rooted in the nature of the virtual photons mediating the transfer process.

In conclusion, we have shown the possibility of altering the strength and the directivity of the matrix element of two

nanostructures by careful engineering of the EM modes and introducing an additional quantum object in the vicinity, hence altering the efficiency of the resonance energy transfer. In addition, the results obtained here can help in the optimization and the design of antenna devices for high efficiency light harvesting and light generation systems.

ACKNOWLEDGMENTS

The work of D.W. is supported by the Monash University Institute of Graduate Research. The work of M.P. is supported by the Australian Research Council, through its Discovery Grant No. DP140100883.

[1] M. Mohseni, P. Rebentrost, S. Lloyd, and A. Aspuru-Guzik, J. Chem. Phys. **129**, 174106 (2008).
[2] B. Valeur and M. Berberan-Santos, *Molecular Fluorescence* (Wiley, Hoboken, NJ, 2012).
[3] R. v. Grondelle and V. I. Novoderezhkin, Nature (London) **463**, 614 (2010).
[4] C. Elisabetta, W. Cathy, W. Krystyna, P. M. G. Curmi, P. Brumer, and G. D. Scholes, Nature (London) **463**, 644 (2010).
[5] M. P. E. Lock, D. L. Andrews, and G. A. Jones, J. Chem. Phys. **140**, 044103 (2014).
[6] D. Sikdar, W. Cheng, and M. Premaratne, J. Appl. Phys. **117**, 083101 (2015).
[7] H. T. Hattori, Z. Li, D. Liu, I. D. Rukhlenko, and M. Premaratne, Opt. Express **17**, 20878 (2009).
[8] D. Sikdar, I. D. R. W. Cheng, and M. Premaratne, J. Opt. Soc. Am. B **30**, 2066 (2013).
[9] D. Sikdar, I. D. Rukhlenko, W. Cheng, and M. Premaratne, Plasmonics **9**, 659 (2014).
[10] C. Rupasinghe, I. D. Rukhlenko, and M. Premaratne, ACS Nano **8**, 2431 (2014).
[11] D. W. Piston and G.-J. Kremers, Trends Biochem. Sci. **32**, 407 (2007).
[12] S. S. Vogel, C. Thaler, and S. V. Koushik, Sci. Signaling **2006**, re2 (2006).
[13] H. Sahoo, J. Photochem. Photobiol. C **12**, 20 (2011).
[14] T. Förster, Ann. Phys. **437**, 55 (1948).
[15] D. L. Andrews and A. A. Demidov, *Resonance Energy Transfer* (Wiley, Hoboken, NJ, 1999).
[16] D. L. Andrews, C. Curutchet, and G. D. Scholes, Laser Photonics Rev. **5**, 114 (2011).
[17] G. D. Scholes, Annu. Rev. Phys. Chem. **54**, 57 (2003).
[18] E. F. James and A. J. Garth, New J. Phys. **16**, 113067 (2014).
[19] D. L. Andrews and D. S. Bradshaw, Eur. J. Phys. **25**, 845 (2004).
[20] D. P. Craig and T. Thirunamachandran, *Molecular Quantum Electrodynamics* (Dover, New York, 1998).
[21] R. P. Feynman, Phys. Rev. **94**, 262 (1954).
[22] R. D. Mattuck, *A Guide to Feynman Diagrams in the Many-Body Problem* (Dover, New York, 1992).
[23] J. S. Avery, Proc. Phys. Soc. **88**, 1 (1966).
[24] L. Gomberoff and E. A. Power, Proc. Phys. Soc. **88**, 281 (1966).
[25] D. L. Andrews, Chem. Phys. **135**, 195 (1989).
[26] G. J. Daniels, R. D. Jenkins, D. S. Bradshaw, and D. L. Andrews, J. Chem. Phys. **119**, 2264 (2003).
[27] D. P. Craig and T. Thirunamachandran, Chem. Phys. **135**, 37 (1989).
[28] G. Juzeliūnas and D. L. Andrews, Phys. Rev. B **49**, 8751 (1994).
[29] G. Juzeliūnas and D. L. Andrews, Phys. Rev. B **50**, 13371 (1994).
[30] A. Salam, J. Chem. Phys. **136**, 014509 (2012).
[31] D. L. Andrews and J. S. Ford, J. Chem. Phys. **139**, 014107 (2013).
[32] R. El-Ganainy and S. John, New J. Phys. **15**, 083033 (2013).
[33] P. L. Hernández-Martínez and A. O. Govorov, Phys. Rev. B **78**, 035314 (2008).
[34] A. Salam, *Molecular Quantum Electrodynamics: Long-Range Intermolecular Interactions* (Wiley, Hoboken, NJ, 2010).
[35] L. Mandel and E. Wolf, *Optical Coherence and Quantum Optics* (Cambridge University Press, Cambridge, UK, 1995).
[36] B. W. van der Meer, in *FRET—Förster Resonance Energy Transfer: From Theory to Applications* (Wiley, Hoboken, NJ, 2013), pp. 23–62.
[37] D. L. Dexter, J. Chem. Phys. **21**, 836 (1953).
[38] R. D. Jenkins, G. J. Daniels, and D. L. Andrews, J. Chem. Phys. **120**, 11442 (2004).
[39] G. J. Daniels and D. L. Andrews, J. Chem. Phys. **117**, 6882 (2002).
[40] F. Frezza, L. Pajewski, D. Saccoccioni, and G. Schettini, Opt. Commun. **265**, 47 (2006).
[41] A. Salam, J. Chem. Phys. **122**, 044112 (2005).
[42] G. D. Scholes and D. L. Andrews, Phys. Rev. B **72**, 125331 (2005).
[43] P. R. Berman, R. W. Boyd, and P. W. Milonni, Phys. Rev. A **74**, 053816 (2006).
[44] P. W. Milonni, R. Loudon, P. R. Berman, and S. M. Barnett, Phys. Rev. A **77**, 043835 (2008).
[45] G. D. Scholes and D. L. Andrews, J. Chem. Phys. **107**, 5374 (1997).